*Korean J. Chem. Eng.*, 35(5), 1065-1072 (2018)
DOI: 10.1007/s11814-018-0008-x

pISSN: 0256-1115
eISSN: 1975-7220

# Effect of slag viscosity model on transient simulations of wall slag flow in an entrained coal gasifier

**Mukyeong Kim, Insoo Ye, and Changkook Ryu†**

School of Mechanical Engineering, Sungkyunkwan University, Suwon 16419, Korea
(*Received 27 July 2017 • accepted 25 January 2018*)

**Abstract**−The viscosity-temperature relation of slag determines its behavior inside an entrained flow coal gasifier. However, existing prediction models give results with large variations among them. We investigated the influence of different viscosity models in the prediction of the steady and transient behaviors of slag flow on the wall of a gasifier undergoing gas temperature changes. Five viscosity models adopted showed differences in the temperature ($T_{250}$) at 25 Pa·s as large as 97 K for the selected slag composition, which was used as the interface temperature between the solid and liquid slag. When the predicted viscosity and corresponding $T_{250}$ increased, the solid slag became thicker and the dynamic response of the slag became slower. In contrast, the differences in the liquid slag thickness were small. The influence of $T_{250}$ predicted was dominant, compared to that of different viscosity curves of the liquid slag.

Keywords: Ash Deposition, Coal Gasification, Entrained Gasifier, Numerical Model, Slag Layer

## INTRODUCTION

In entrained coal gasifiers, the operating temperatures are typically well above the ash melting point, and a significant fraction of the molten ash is deposited on the wall to form a slag layer [1]. The slag layer is intended to protect the refractory [2,3] and facilitate the ash discharge by gravity [4]. However, too thick a slag layer may lead to blockage at the slag tap, which is a major operational problem. This can be caused by high slag viscosity, due to a decrease in gas temperatures (e.g., because of the low calorific value of coal) or by changes in ash composition. Because the slag thickness and gas temperature are very difficult to measure directly, it is crucial to control the coal quality and to monitor the operating conditions of the gasifier. For water-cooled gasifiers, the heat transfer rate to the coolant on the wall and the syngas composition downstream are used to estimate the gas temperature and slag thickness, despite the time delays and uncertainties associated with the complexity of the phenomena.

With respect to the slag behavior, the most important property is the viscosity-temperature relation [5], which is determined by a complicated interaction and transformation of the ash components. Further, the slag viscosity, which is very sensitive to temperature, increases logarithmically with decreasing temperatures. When the slag reaches a particular temperature during cooling, certain slags begin to exhibit non-Newtonian fluid behavior and viscosity rises sharply because of crystallized mineral formation [6]. This temperature is referred to as the critical viscosity temperature ($T_{cv}$). $T_{cv}$ can be obtained through measurement, but it may be difficult to determine depending on the slag types [7]. There are various $T_{cv}$ correlations based on slag composition and ash fusion temperatures for modeling and design evaluation [8], but the value at a viscosity of 25 Pa·s is generally used [9]. In contrast, glassy slags with high silica content have a continuous increase in viscosity without $T_{cv}$ [7,10]. In slag flow modeling, the temperature ($T_{250}$) at 25 Pa·s (250 poise) is considered as the interface value between the solid (immobile) and liquid (mobile) slag layers [11-14].

In parallel with the experimental characterization of the slag properties and phase transformation, several researchers have developed models to predict slag viscosity. Most models use semi-empirical correlations with coefficients calculated from the chemical composition of major minerals, assuming that the liquid slag is a Newtonian fluid. These include the Urbain et al. [15], S2 correlation [16], Watt and Fereday [17], Browning et al. [18], and Kalmanovitch and Frank models [19]. These models have errors of about 30% for a limited range of slag composition, which is comparable to the experimental reliability [20]. However, their reliability is low outside that range. Further, the viscosity characteristics of the slag phase at low temperatures are not reflected in those models [21]. Kondratiev and Jak [22] modified the slag viscosity calculation method to improve its accuracy in the low temperature region by calculating separately the homogeneous and heterogeneous slag viscosities. Saxén [23] introduced an artificial neural network model using slag viscosity data to investigate the interactions between variables, obtaining better results than the conventional models in the low viscosity region (0-6 Pa·s). Duchesne [6,24] improved the artificial neural network model for viscosity prediction in wider ranges of temperature and composition.

To understand the slag flow behavior on the gasifier wall, several models or CFD-based simulations have been proposed. Analytical slag models, such as Seggiani [11,25] and Yong et al. [12,26], estimate the slag thickness and heat transfer to the wall using algebraic equations acquired from the integration of the mass, momentum, and enthalpy conservation equations for the liquid slag region. In the models, the viscosity-temperature relation is assumed to have

†To whom correspondence should be addressed.
E-mail: cryu@me.skku.ac.kr

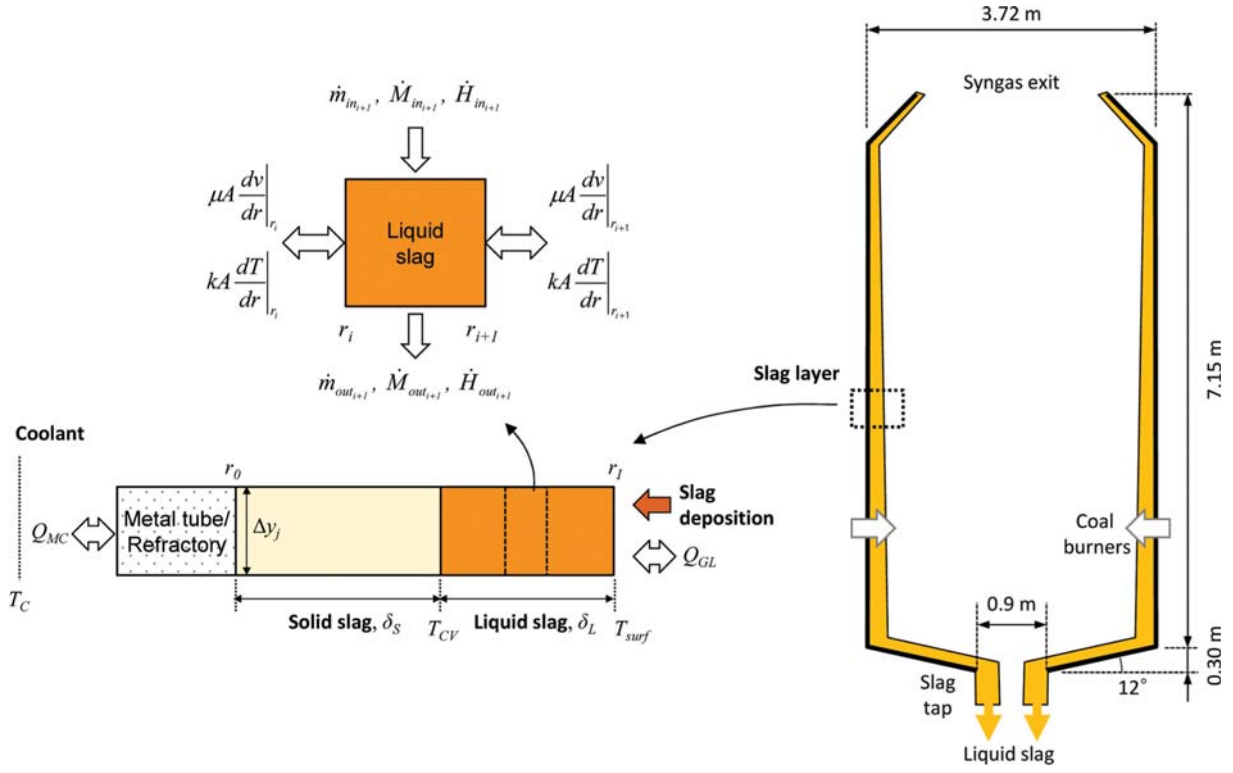


**Fig. 1. Schematic of the modeling approach for the slag layer and geometry of the target gasifier.**

the specific form of $\mu$=aTexp(b/T). Further, the temperature of the liquid slag layer is assumed to have a linear [11] or cubic profile [12] so that $\mu$(T) in the momentum equation becomes $\mu$(x) for direct integration. On the other hand, Ye and Ryu [27] developed a numerical model based on the discretization of the governing equations, which does not require the assumption on the temperature profile and can adopt various viscosity models. It has been recently expanded to a transient model in the authors' previous study [28], and the dynamic behavior of the slag layer has been investigated. These models can be coupled with a one-dimensional process model or computational fluid dynamic simulation for the coal and gas regime as boundary condition for the wall [14,29-31].

As discussed, various viscosity models have been proposed in the literature, and the predicted values for a particular slag often exhibit significant variations among the models and from the measured data. Our aim was to evaluate how much the choice of a specific viscosity model influences the steady-state values and dynamic behavior of the slag layer in the slag flow model. Among the various viscosity models, five frequently used models were applied to the transient slag model for an entrained flow coal gasifier simulating the following gas temperature changes: 1) increase from 1,800 to 1,900 K, and 2) decrease from 1,800 to 1,700 K. The initial and final steady-state results were characterized by the slag thickness at the slag tap, total heat transfer rate to the coolant, and velocity and temperature profiles in the slag layer. The dynamic behavior was quantified by the characteristic times for change in the slag thickness and heat transfer rate, and the differences were compared among the viscosity models. In particular, the effects of different $T_{250}$ values predicted by the viscosity models were assessed in detail.

## TRANSIENT MODELING OF SLAG LAYER

### 1. Governing Equations and Numerical Method

The transient slag flow model was presented in detail in our previous study [28]. Therefore, it is briefly summarized here. The modeling approach for the slag layer on the wall of an entrained gasifier is depicted in Fig. 1. The surface of the liquid slag is exposed to heat transfer with the hot syngas ($Q_{GL}$) and deposition of slag ($m_{dep}$), while the colder solid slag facing the wall has thermal conduction to the refractory and ultimately to the coolant ($Q_{MC}$). For the transient flow modeling, the slag layer is divided into control volumes in the streamwise direction along the wall (index j), and in the perpendicular direction (index i), including the metal tube and refractory sections. The slag deposition on the liquid slag surface is treated as the formation of a new control volume. The transformation between solid and liquid slag is considered using $T_{250}$ as the interface temperature for changes in temperature during the transient period.

Table 1 lists the governing equations for the slag layer, which are converted into discretized equations for the 2-dimensional control volumes. The coupled linear system of variables was solved iteratively to determine the thickness, temperature, velocity, viscosity, and heat transfer in each control volume. The model was programmed using Microsoft Excel with the Visual Basic application. In the transient calculation, the steady-state solution for the initial condition was established first. Subsequently, the solution continued for each time step until it reached the final steady state, for given changes in the operating conditions.

### 2. Simulation Conditions and Methods

The target in this study was the Prenflo gasifier at the Puertol-

**Table 1. Governing equations of mass, momentum, and energy conservation for the slag layer**

| Variables/Terms | Equations |
|---|---|
| Mass conservation | $\frac{dm}{dt}=\dot{m}_{in}-\dot{m}_{out}+\dot{m}_{dep}$ |
| Momentum conservation | $\frac{dM}{dt}=\dot{M}_{in}-\dot{M}_{out}+\left(\mu A_{r+dr}\frac{dv}{dr}\Big\|_{r+dr}-\mu A_r\frac{dv}{dr}\Big\|_r\right)+\rho g\sin\alpha\cdot dV+\dot{M}_{dep}$ |
| Energy conservation | $\frac{dH}{dt}=\dot{H}_{in}-\dot{H}_{out}+kA_{r+dr}\frac{dT}{dt}_{r+dr}-kA_r\frac{dT}{dr}_r+Q_{MC}+Q_{GL}+\dot{H}_{dep}$ |
| Slag layer cross-section area | $A_r=2\pi r\Delta y\sin\alpha$ |
| Deposit slag enthalpy | $\dot{H}_{dep}=\dot{m}_{dep}C_p(T_{dep}-T_{ref})$ |
| Total heat transfer to the slag | $Q_{GL}=A_{surf}[h_{conv}(T_{gas}-T_{surf})+\varepsilon\sigma(T_{gas}^4-T_{surf}^4)]$ |
| Total heat transfer to the wall | $Q_{MC}=h_CA_C(T_M-T_C)$ |

lano IGCC plant in Spain, as illustrated in Fig. 1, which was used in previous investigations on slag behavior [11,27,28]. Its cylindrical body has a diameter of 3.72 m, with four coal burners on the sidewall, and the syngas produced is transferred to the cooling section through the exit at the top. In the lower part, the bottom cone is narrowed to an angle of 12°, to turn the coal and gas flows upward while collecting the liquid slag and discharging it through the slag tap below.

Table 2 summarizes the initial operating conditions of the gasifier and the slag composition, which were taken from previous studies [28]. The gasifier was assumed to have a uniform gas temperature ($T_{gas}$) of 1,800 K at the initial state. Subsequently, it was subjected to an instantaneous increase to 1,900 K, or an instantaneous decrease to 1,700 K to analyze the slag behaviors influenced by various viscosity models. The slag deposits on the wall maintained a uniform mass flux at a total of 5 kg/s, while the deposition temperature was assumed to be 50 K below $T_{gas}$. The density, thermal conductivity, specific heat, and emissivity of the slag were

**Table 2. Operating condition of the gasifier and slag properties prescribed in this study**

| Model parameter | | Reference value/model |
|---|---|---|
| Gas temperature | | 1) 1,800 K (initial)→1,900 K<br>2) 1,800 K (initial)→1,700 K |
| Slag composition | | $SiO_2$ 44.24%, CaO 24.27%, $Al_2O_3$ 22.05%, $Fe_2O_3$ 3.39%, $SiO_3$ 2.29%, MgO 1.30%, $TiO_2$ 0.96%, $K_2O$ 0.52%, $Na_2O$ 0.22%, others 0.75% |
| Slag deposition | Temperature | $T_{gas}$ - 50 K |
| | Mass rate | 5.0 $kg\cdot s^{-1}$ (uniform mass flux) |
| Slag properties | Density | 2506.99 $kg\cdot m^{-3}$ |
| | Emissivity | 0.83 |
| | Thermal conductivity | Liquid: 1.58 $W\cdot m^{-1}\cdot K^{-1}$<br>Solid: $1.040+2.025\times10^{-4}T-0.246/T^2$ $W\cdot m^{-1}\cdot K^{-1}$ |
| | Specific heat | Liquid: 1.40 $kJ\cdot kg^{-1}\cdot K^{-1}$<br>Solid: $0.922+1.796\times10^{-4}T-0.218/T^2$ $kJ\cdot kg^{-1}\cdot K^{-1}$ |
| Coolant (water) | Convection coefficient | $1\times10^4$ $W\cdot m^{-2}\cdot K^{-1}$ |
| | Temperature | 523 K |

**Table 3. Correlations of selected viscosity models and coefficients calculated using slag composition**

| Model | Viscosity equation | Coefficients | $T_{250}$ (K) |
|---|---|---|---|
| Urbain | $\eta=aTe^{1000b/T}$ | $a=1.433\times10^{-8}$, b=23.723 | 1455.4 |
| Watt & Fereday | $\log\eta=\frac{10^7 m}{(T-150)^2}+c$ | m=0.418, c=−1.0421 | 1525.4 |
| S2 correlation | $\log\eta=4.468\left(\frac{S}{100}\right)^2+1.265\left(\frac{10^4}{T}\right)-7.44$ | S=60.44 | 1541.6 |
| Kalmanovitch & Frank | $\eta=aTe^{1000b/T}$ | $a=3.27\times10^{-10}$, b=27.421 | 1547.9 |
| Browning | $\log\left(\frac{\eta}{T-T_s}\right)=\frac{14788}{T-T_s}-10.931$ | $T_s$=−69.7147 | 1552.0 |

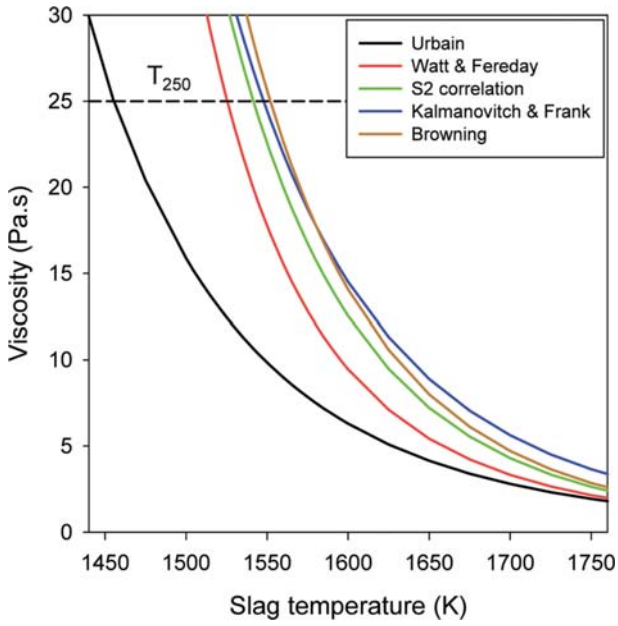


**Fig. 2. Slag viscosity vs. temperature predicted by the selected viscosity models.**

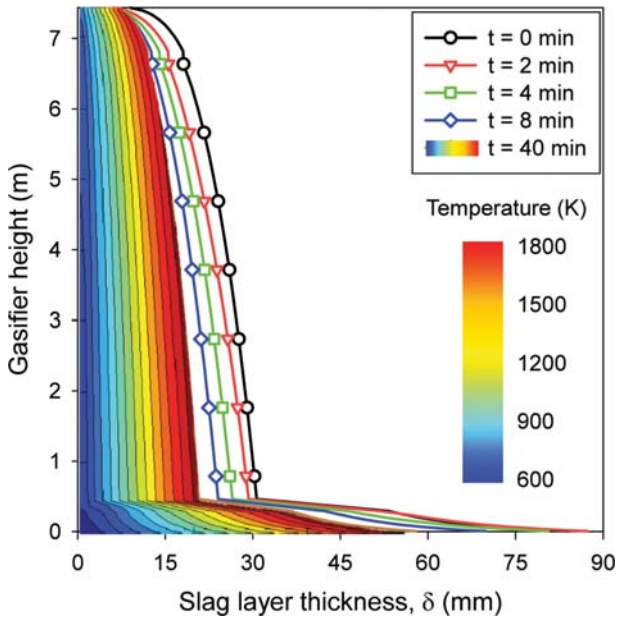


**Fig. 3. Change in slag thickness and temperature contour at the final steady state by increase in $T_{gas}$ for KF model.**

calculated using the respective models available in the literature [32,33] for the elemental composition listed in Table 2. According to Zhang et al. [34], the solid slag may have a porosity as high as 10%, which lowers the thermal conductivity by up to 5%. However, it was not considered in this study because the changes in the thermal conductivity have a minor impact on the slag thickness [35].

Table 3 presents the viscosity equation and coefficients calculated using the slag composition for five viscosity models, the Urbain (Ur), S2 correlation (S2), Watt & Fereday (WF), Browning (Br), and Kalmanovitch & Frank (KF) models. Fig. 2 plots the slag viscosity predicted by the models. For each model, $T_{250}$ was determined for the viscosity of 25 Pa·s as the interface value between the solid and liquid slag layers. The Ur model provides the lowest viscosity with $T_{250}$ of 1,455.4 K, whereas the S2, KF, and Br models predict similar values with $T_{250}$ ranging between 1,541.6 and 1,552.0 K. The KF model gives a $T_{250}$ of 1,547.9 K, but the viscosity in the liquid slag regime decreases slower than in the other models, and it becomes the highest above 1,580 K. In contrast, the WF model has a $T_{250}$ of 1,525.4 K, close to that of the S2 model, but decreases rapidly at higher temperatures, thus approaching the values of the Ur model. Such differences in $T_{250}$ and the viscosity-temperature relation for the liquid slag would influence the steady state and transient behavior of the slag layers, which are the focus of this study.

## RESULTS AND DISCUSSION

### 1. Dynamic Response of the Slag Layer and Heat Transfer to the Wall

In this section, the steady-state results and dynamic responses of the slag layer to the increase in $T_{gas}$ from 1,800 to 1,900 K are explained using the KF model as the reference case. Fig. 3 shows the change in slag thickness caused by the increase in $T_{gas}$ and the temperature distribution at the final steady state. The slag temperature increases gradually between the water-cooled wall and the hot syngas. Near the surface facing the syngas, the liquid slag (above $T_{250}$ of 1,547.9 K) flows downward due to gravity. This layer also acts as a thermal resistance against heat transfer to the solid slag and the wall. With continuous deposition of new slag from the gas regime, the liquid slag gradually becomes thicker toward the slag tap at the bottom. At the same time, this increases the solid slag thickness. At the bottom cone (y≤0.3 m), the slag layer rapidly becomes very thick because of the sudden change in wall angle, and the corresponding decrease in gravity.

When $T_{gas}$ increases from 1,800 to 1,900 K, the increase in the slag temperature moves the liquid-solid interface at $T_{250}$ closer to the wall, and part of the solid slag facing the liquid slag gradually turns into a liquid, flowing down. At the same time, the viscosity of the liquid slag becomes lower, causing a velocity increase. As a result, both the liquid and solid slag layers become thinner. Such changes occur faster in the upper part of the gasifier, whereas those in the bottom cone are slower because of the existing thick slag layer and the increased downward flow of liquid slag. Despite the differences in the response rate along the streamwise direction, further analysis of the slag layer thickness hereafter will be focused at the slag tap (y=0), which is the point of interest for prevention of blockage.

Fig. 4 shows the changes in the wall heat flux and surface temperature ($T_{surf}$) of the liquid slag. The response of $T_{surf}$ to the increase in $T_{gas}$ is almost immediate, increasing from 1,770 K at the slag tap at the initial steady state to 1,860 K at t=2 min. The change in $T_{surf}$ becomes very small thereafter. In contrast, the heat flux exhibits a gradual increase, because the increase in slag temperature is rapid only near the liquid slag surface at the early stages, which makes the temperature profile deviate from the linear relationship [28]. Therefore, the temperature gradient in the outer solid slag requires a longer time to increase. This is accompanied by the gradual

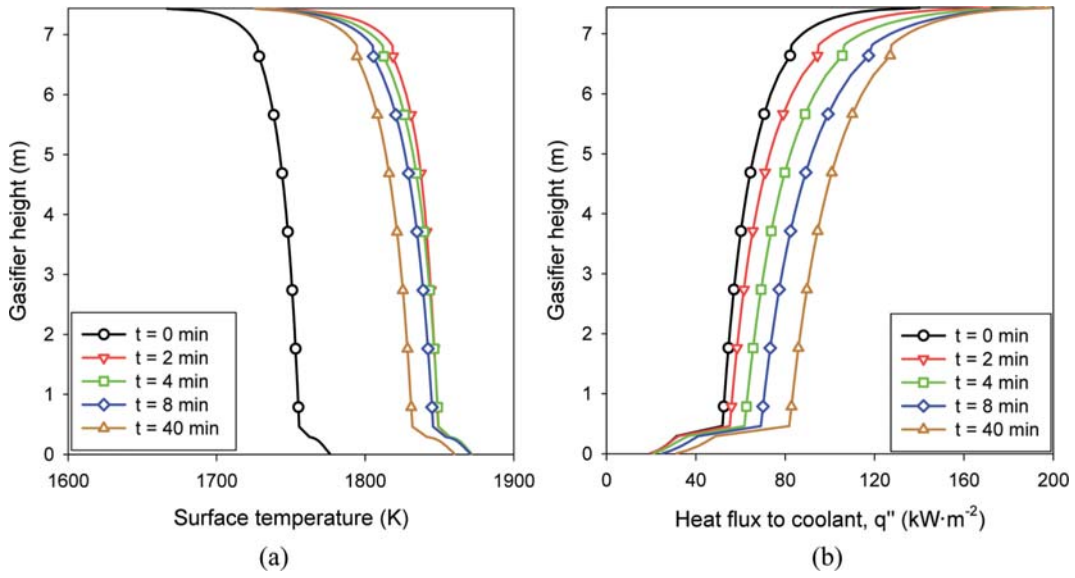


**Fig. 4. Changes in (a) the surface temperature of the liquid slag and (b) the wall heat flux by increase in $T_{gas}$ for KF model.**

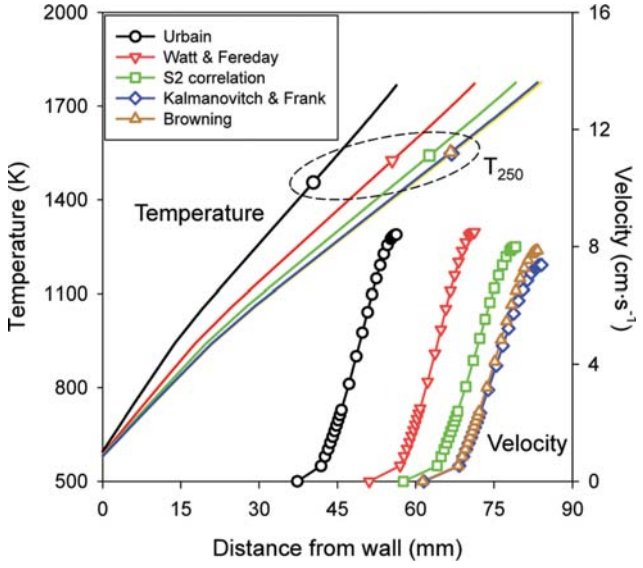


**Fig. 5. Profiles of slag temperature and velocity at the slag tap at the initial state for different viscosity models.**

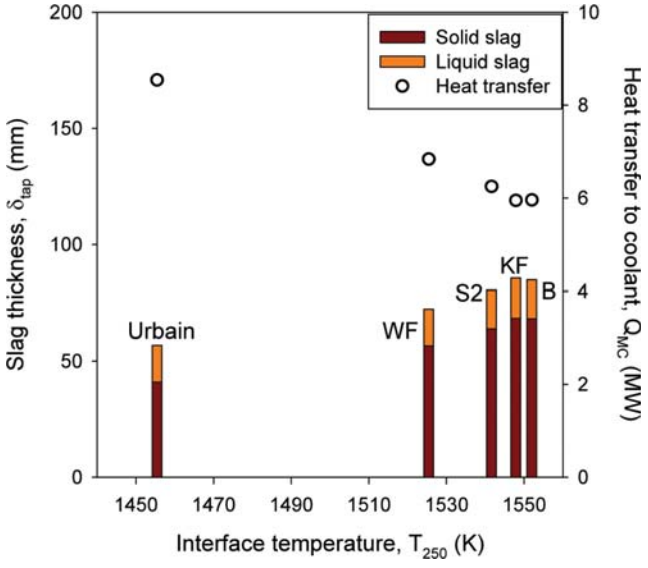


**Fig. 6. Slag thickness at slag tap and heat transfer to the wall at the initial state for different viscosity models.**

transformation of solid slag to liquid, reducing the slag thickness.

**2. Influence of Slag Viscosity Model: Initial Steady State**

Fig. 5 compares the temperature and velocity profiles of the slag layer at the slag tap for the initial steady state (t=0 min) as predicted by the different viscosity models. The slag thickness differs significantly among the models, ranging between 56.3 mm (Ur model) and 84.1 mm (Br model). With the two boundary temperatures ($T_{surf}$ and $T_{r0}$) similar in the models, the temperature gradient varies correspondingly. The Ur model gives the smallest slag thickness, and predicts the lowest slag viscosity and $T_{250}$, as shown in Fig. 2. In contrast, the result of the Br model has the largest slag thickness, closely followed by that of the KF model. This also is in agreement with the viscosity-temperature curves in Fig. 2.

In the velocity profiles of the liquid slag, also plotted in Fig. 5, the surface values are about 8 cm/s because of the higher temperatures and corresponding decreases in viscosity. Although the difference is small, the KF model results in the lowest surface velocity, whereas the Ur and WF models give larger values. This corresponds well with the viscosity predicted at $T_{surf}$ (~1,750 K) shown in Fig. 2. Overall, the velocity profiles are similar between the models because the flow rate of liquid slag is identical (equal to the total deposition rate of 5 kg/s). For the same reason, the liquid slag thickness also becomes similar between models.

To analyze the influence of $T_{250}$, the slag thickness at the slag tap ($\delta_{tap}$) and total heat transfer rate to the coolant ($Q_{MC}$) are plotted for the $T_{250}$ predicted by the models in Fig. 6. A higher $T_{250}$ leads to thicker solid slag and lower $Q_{MC}$. Note that the solid slag thickness is inversely proportional to the heat flux ($q \sim (T_{250}-T_{wall})/\delta_S$). In

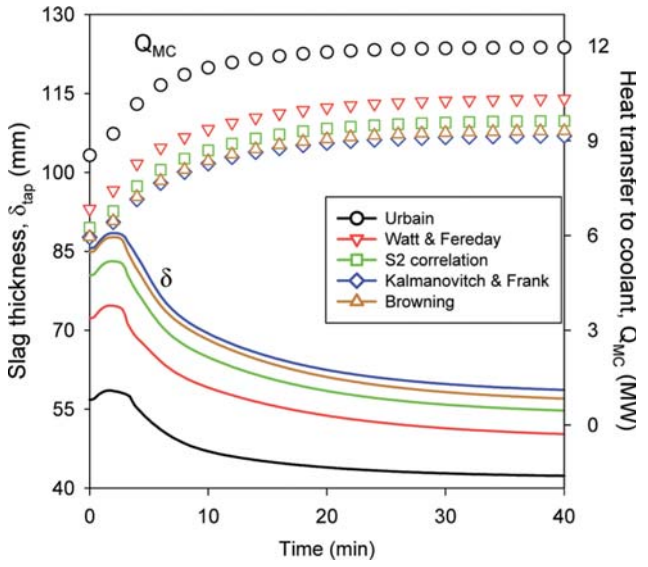


**Fig. 7. History of slag thickness at the slag tap and heat transfer rate to the coolant by increase in $T_{gas}$ from 1,800 to 1,900 K.**

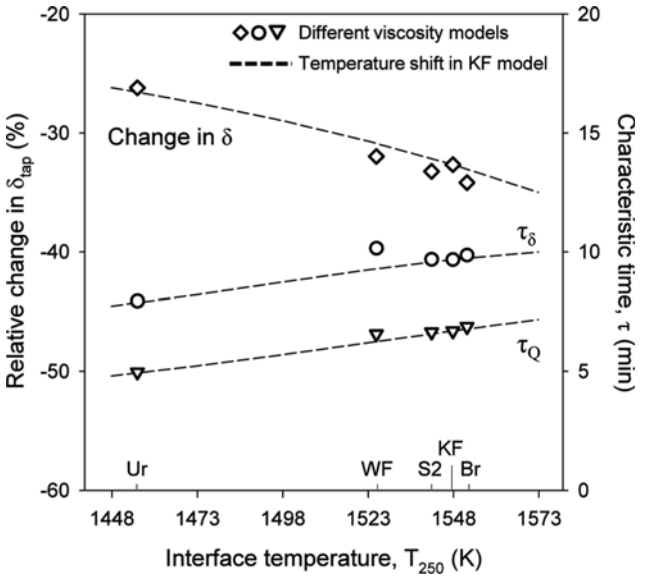


**Fig. 8. Changes in the slag thickness and characteristic times vs. $T_{250}$ for increase in $T_{gas}$ from 1,800 to 1,900 K.**

contrast, the liquid slag has similar thicknesses as mentioned previously. It is noticeable that the KF model gives a slightly larger slag thickness than that of the Br model. The reason is that the viscosity of the KF model is larger than that of the Br model at higher temperatures (Fig. 2), which lowers the surface velocity (Fig, 5).

### 3. Influence of Slag Viscosity Model: Dynamic Behavior for Increase in $T_{gas}$

Fig. 7 shows the dynamic behavior of the slag layer in terms of the slag thickness and total $Q_{MC}$ for the increase in $T_{gas}$ to 1,900 K. The trends are similar between the viscosity models, although the initial and final values are different. For the first few minutes, the slag layer becomes thicker by the phase change within part of solid slag into liquid, which results in an increase in the liquid flow rate at the slag tap. Then, $\delta_{tap}$ gradually stabilizes to a new steady state. In contrast, $Q_{MC}$ integrated for the entire wall undergoes a rapid increase in the initial stage by the increase in $T_{gas}$ and thinning of the slag layer, except for the lower part of the gasifier. It also stabilizes faster than $\delta_{tap}$.

To express quantitatively the dynamic responses between the models, the respective characteristic times are calculated for 63.2% change in $\delta_{tap}$ ($\tau_\delta$) and for the total $Q_{MC}$ ($\tau_Q$), as listed in Table 3. The trends are consistent between the viscosity models, but the models with higher $T_{250}$ values lead to larger characteristic times (i.e., slower changes), and larger changes in $\delta_{tap}$ and $Q_{MC}$. For example, $\tau_\delta$ of Br model (10.35 min) is 2 min longer than that of the Ur model (8.32 min). The reasons for the slower changes are i) the solid slag is initially thicker, as shown in Fig. 6 (the change by the increase in $T_{gas}$ is initially limited to the liquid surface region and then it slowly penetrates deeper into the inner slag layer [28]), and ii) the viscosity is larger so that the liquid slag flow becomes slower. $\tau_Q$ is approximately 4 min shorter than $\tau_\delta$, which suggests that the heat absorption by the coolant could be an indicator for the gasifier temperature and slag thickness, preceding the change in $\delta_{tap}$.

### 4. Effect of Different $T_{250}$ Values

In the results obtained thus far, the viscosity models effect the slag behavior by the differences in $T_{250}$ and viscosity curves in the liquid slag regime. To clarify the contribution of these two factors, the viscosity curve and the corresponding $T_{250}$ were shifted for the KF model and the simulations were repeated. The shift in viscosity was achieved by adding a constant c in the term for temperature, as follows.

$$\eta = a(T-c)e^{1000b/(T-c)}$$

Considering that $T_{250}$ of the five viscosity models ranges between 1,455 and 1,552 K, the constant c in the above equation varied from −100 to 25 K, so that the resultant $T_{250}$ values ranged between 1,447.9 and 1,572.9 K. The viscosity curves were also shifted by the constant, maintaining the same slopes of the liquid slag regime in

**Table 4. Summary of dynamic behaviors predicted using different viscosity models for increase in $T_{gas}$ from 1,800 to 1,900 K**

| Viscosity model | $T_{250}$ (K) | Relative change (%) in $\delta_{tap}$ | $\tau_\delta$ (min) | Relative change (%) in $Q_{MC}$ | $\tau_Q$ (min) |
|---|---|---|---|---|---|
| Urbain | 1455.4 | −23.7 | 8.32 | 32.8 | 4.43 |
| Watt & Fereday | 1525.4 | −28.9 | 10.29 | 43.9 | 6.13 |
| S2 correlation | 1541.6 | −29.9 | 10.17 | 46.8 | 6.63 |
| Kalmanovitch & Frank | 1547.9 | −29.3 | 10.02 | 46.7 | 6.81 |
| Browning | 1552.0 | −30.8 | 10.35 | 50.0 | 6.81 |

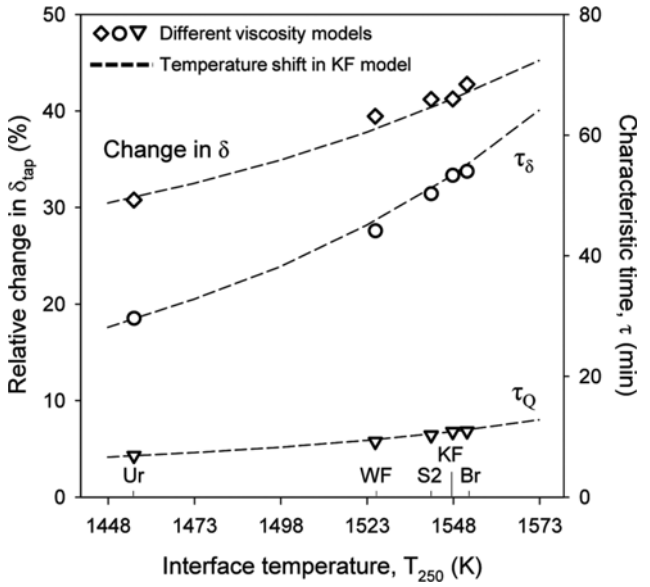


**Fig. 9. Changes in the slag thickness and characteristic times vs. $T_{250}$ for decrease in $T_{gas}$ from 1,800 to 1,700 K.**

Fig. 2 for the KF model.

Fig. 8 compares the key results between the five viscosity models (symbols) and KF model with the temperature shifts (dotted line) for the increase in $T_{gas}$. The results using the KF model with the temperature shifts are very close to the values from the viscosity models, confirming that $T_{250}$ is the dominant factor. The deviations between the two methods are attributable to the different viscosity curves in the liquid slag regime, which are small.

Shown in Fig. 9 are the results for the decrease in $T_{gas}$ from 1,800 to 1,700 K. $\delta_{tap}$ becomes thicker by the corresponding increase in the slag viscosity, in which the viscosity models with higher $T_{250}$ predict much thicker $\delta_{tap}$ and slower changes to the final steady state. For example, the Ur model predicts the final value of $\delta_{tap}$ to increase by 30.8% (from 56.8 mm to 82.1 mm), and the Br model to increase by 42.8% (from 84.9 mm to 148.3 mm). $\tau_\delta$ is also 24.5 min larger in the Br model. Therefore, the effect of the viscosity model becomes more significant when $T_{gas}$ decreases and the effect of $T_{250}$ is still dominant over the different viscosity curves in the liquid slag regime. On the other hand, $\tau_Q$ is about 11 min or lower, which is much smaller than $\tau_\delta$, because $\tau_Q$ refers to the entire wall, which has fast response by the increase in slag thickness and thermal resistance to heat transfer. In contrast, $\delta_{tap}$ is at the slag tap, which requires longer time for the slag above to settle down to the new steady state, including the transformation of the inner liquid slag to solid. Such difference in $\tau_Q$ and $\tau_\delta$ gives emphasis to the importance of monitoring the wall heat transfer rate.

## CONCLUSIONS

We investigated the influence of various slag viscosity models on the prediction of the steady and transient behaviors of the slag flow on the wall of an entrained flow coal gasifier, undergoing a gas temperature increase from 1,800 to 1,900 K. The viscosity models evaluated were the Kalmanovitch and Frank, Urbain, Watt and Fereday, S2 correlation, and Browning models, all of which are based on the ash composition. The key findings are as follows.

- The five viscosity models had significant variations among them in $T_{250}$ (at 25 Pa·s), as large as 97 K for the selected slag composition, which emphasizes the importance of determining the viscosity-temperature correlation by measurement.
- When the predicted slag viscosity and $T_{250}$ increased, the solid slag formed between the cold refractory and liquid slag became thicker. This also slowed down the dynamic response of the slag, increasing the characteristic time required for the slag thickness and heat transfer rate to the wall to reach a new steady state by gas temperature change.
- In contrast, the differences in the liquid slag thickness were small, because the down flow of liquid slag was concentrated in the narrow region near the surface facing the hot gas regime.
- The effect of $T_{250}$ predicted by the models was dominant, compared to the viscosity-temperature relation in the liquid slag regime.
- The influence of the viscosity model was more significant when the gas temperature decreased.

Although we focused on identifying the influence of the viscosity models, the results can also be interpreted as the effect of slag composition, which leads to different viscosity curves and $T_{250}$ values. Additionally, we only considered the response in the slag flow by assuming uniform and fixed gas temperature distribution, without taking the interaction between the two regimes into account. Further studies are required to develop a process model for the gasifier with the slag flow model coupled as the boundary condition.

## ACKNOWLEDGEMENT

This work was supported by the Establishment and Utilization of Clean Fuel Test Bed project funded by the Korea Institute of Energy Technology Evaluation and Planning (KETEP) affiliated with the Ministry of Knowledge Economy of the Korean Government (No. 20152010201970).

## SYMBOLS

a : coefficient
b : coefficient
$C_P$ : specific heat of the slag [$J \cdot kg^{-1} \cdot K^{-1}$]
g : gravity [9.81 $m/s^2$]
H : enthalpy [J/s]
h : convection coefficient [$W \cdot m^{-2} \cdot K^{-1}$]
k : thermal conductivity [$W \cdot m^{-2} \cdot K^{-1}$]
M : momentum [$kg \cdot m \cdot s^{-2}$]
m : mass flow rate [$kg \cdot s^{-1}$]
Q : heat transfer rate [W]
r : radius perpendicular to the wall [m]
T : temperature [K]
V : volume [$m^3$]
v : streamwise velocity [$m \cdot s^{-1}$]
Δy : height of control volume parallel to the wall [m]

### Greek Letters

$\alpha$ : angle from the horizontal plane [°]

$\delta$ : thickness of slag layer [m]
$\varepsilon$ : emissivity
$\mu$ : viscosity [Pa·s]
$\rho$ : density [kg·m$^{-3}$]
$\sigma$ : Stefan-Boltzmann constant

**Subscripts**

C : coolant (water)
cv : critical viscosity
dep : depositing slag
gas : gas
GL : from gas to liquid slag
I : innermost control volume facing the gas
i : index for a control volume within a section of slag layer
in : inflow
j : index for a section of slag layer in the streamwise direction
L : liquid slag
M : metal tube
MC : from metal tube to coolant
out : outflow to the section below
ref : reference temperature
S : solid slag
surf : liquid slag surface facing syngas
tap : at the slag tap
wall : entire gasifier wall

## REFERENCES


1. L. D. Smoot and P. J. Smith, *Coal combustion and gasification*, Springer Science & Business Media (2013).
2. T. K. Kaneko, J. P. Bennett and S. Sridhar, *J. Am. Ceram. Soc.*, **94**, 4507 (2011).
3. G. N. Shannon, P. L. Rozelle, S. V. Pisupati and S. Sridhar, *Fuel Process. Technol.*, **89**, 1379 (2008).
4. W. Song, Y. Sun, Y. Wu, Z. Zhu and S. Koyama, *AIChE J.*, **57**, 801 (2011).
5. C. Higman and S. Tam, *Chemical Reviews*, **114**, 1673 (2013).
6. M. A. Duchesne, A. Macchi, D. Y. Lu, R. W. Hughes, D. McCalden and E. J. Anthony, *Fuel Process. Technol.*, **91**, 831 (2010).
7. M. Oh, D. Brooker, E. De Paz, J. Brady and T. Decker, *Fuel Process. Technol.*, **44**, 191 (1995).
8. S. Vargas, *Straw and coal ash rheology*, Department of Chemical Engineering, Technical University of Denmark (2001).
9. J. Wang, H. Liu, Q. Liang and J. Xu, *Fuel Process. Technol.*, **106**, 704 (2013).
10. K. C. Mills, L. Yuan and R. T. Jones, *J. South. Afr. Inst. Min. Metall.*, **111**, 649 (2011).
11. M. Seggiani, *Fuel*, **77**, 1611 (1998).
12. S. Z. Yong and A. Ghoniem, *Fuel*, **97**, 457 (2012).
13. D. Bi, Q. Guan, W. Xuan and J. Zhang, *Fuel*, **150**, 565 (2015).
14. R. F. Monaghan and A. F. Ghoniem, *Fuel*, **91**, 61 (2012).
15. G. Urbain, *Trans. J. Br. Ceram. Soc.*, **80**, 139 (1981).
16. W. T. Reid, *External corrosion and deposits: Boilers and gas turbines*, Fuel and Energy Science Series; American Elsevier Publishing Co., New York (1971).
17. J. Watt and F. Fereday, *J. Inst. Fuel*, **42**, 99 (1969).
18. G. Browning, G. Bryant, H. Hurst, J. Lucas and T. Wall, *Energy Fuel*, **17**, 731 (2003).
19. D. P. Kalmanovitch and M. Frank, *An effective model of viscosity for ash deposition phenomena*, Proceedings of mineral matter and ash deposition from coal, 22 (1988).
20. K. Mills, *Estimation of physicochemical properties of coal slags and ashes*, ACS Publications (1986).
21. S. Vargas, F. Frandsen and K. Dam-Johansen, *Elsam-idemitsu kosan cooperative research project: Performance of viscosity models for high-temperature coal ashes*, Department of Chemical Engineer-ing, Technical University of Denmark, CHEC Report (1997).
22. A. Kondratiev and E. Jak, *Fuel*, **80**, 1989 (2001).
23. H. Saxén and X. Zhang, *Neural-network based model of blast furnace slag viscosity*, Proceedings of the International Conference on Engineering Application of Neural Networks, 167 (1997).
24. M. A. Duchesne, A. M. Bronsch, R. W. Hughes and P. J. Masset, *Fuel*, **114**, 38 (2013).
25. M. Seggiani, *Fuel*, **78**, 1121 (1999).
26. S. Z. Yong, M. Gazzino and A. Ghoniem, *Fuel*, **92**, 162 (2012).
27. I. Ye and C. Ryu, *Fuel*, **150**, 64 (2015).
28. M. Kim, I. Ye and C. Ryu, *Fuel*, **196**, 532 (2017).
29. C. Kim, R. Kim, Z. Wu and C. Jeon, *Korean J. Chem. Eng.*, **33**, 1767 (2016).
30. H. Lee, J. Lee, Y. Joo, M. Oh and C. Lee, *Appl. Energy*, **131**, 425 (2014).
31. Z. Yang, Y. Xue, Y. Wu, Z. Wang, Z. Li and W. Ni, *Chem. Eng. Process. Process Intensif.*, **74**, 131 (2013).
32. K. C. Mills and J. M. Rhine, *Fuel*, **68**, 193 (1989).
33. K. C. Mills and J. M. Rhine, *Fuel*, **68**, 904 (1989).
34. B. Zhang, Z. Shen, D. Han, Q. Liang, J. Xu and H. Liu, *Appl. Therm. Eng.*, **112**, 1178 (2017).
35. I. Ye, J. Oh and C. Ryu, *Energies*, **8**, 3370 (2015).